Computational Analysis of Seismic Waves Attenuation Caused by Porosity Variability in a Fluid-Saturated Porous Model of Thawing Permafrost

Galina Reshetova[1(✉)], Mikhail Novikov[2], and Evgeniy Romenski[3]

[1] Institute of Computational Mathematics and Mathematical Geophysics SB RAS, Novosibirsk 630090, Russia
kgv@nmsf.sscc.ru

[2] Trofimuk Institute of Petroleum Geology and Geophysics SB RAS, Novosibirsk 630090, Russia
novikovma@ipgg.sbras.ru

[3] Sobolev Institute of Mathematics SB RAS, Novosibirsk 630090, Russia
evrom@math.nsc.ru

Abstract. A computational model for wave fields simulation in a saturated deformable porous medium is presented. The governing differential equations of the model are derived from a general Symmetric Hyperbolic Thermodynamically Compatible (SHTC) two-phase model of saturated porous medium and form a linear PDE system allowing the application of an efficient finite difference method on a staggered grid. A series of numerical test problems showed a strong dependence of wave attenuation on porosity and relaxation time coefficient. It was also shown that the constitutive equations of the SHTC give a constant value of the quality factor over a range of seismic frequencies, making it possible to use the SHTC model to develop seismic methods for monitoring permafrost thaw.

Keywords: Wave field simulation · Fluid saturated porous medium · Quality factor · Staggered grid finite difference scheme

1 Introduction

In recent years, there has been growing interest in the development of methods for seismic monitoring of permafrost thawing, caused, in particular, by global warming. These studies are undoubtedly important since soil thawing leads to a loss of its bearing capacity and, as a result, can lead to catastrophic consequences, such as the destruction of buildings and communications. Therefore, a particularly important task is the development of seismic monitoring methods that make it possible to characterize changes in the physical properties of

This work was financially supported by the Russian Science Foundation, grant No. 22-11-00104.

© The Author(s), under exclusive license to Springer Nature Switzerland AG 2024
O. Gervasi et al. (Eds.): ICCSA 2024 Workshops, LNCS 14817, pp. 321–333, 2024.
https://doi.org/10.1007/978-3-031-65238-7_22

permafrost depending on changes in wave fields with changes in ambient temperature [1–3].

Seismic monitoring is based on the analysis of wave fields, their propagation and reflection in the upper layers of the Earth's crust, including areas of permafrost, which from the point of view of continuum mechanics is a complex geological deformable medium. The variability of wave fields in response to external conditions can be used to assess changes in permafrost zones and predict critical events. As temperatures rise in permafrost zones, ice melts, forming a porous structure that can contain water and gases as a result of melting. To describe the complex structure of the permafrost zone under the influence of temperature, a mathematical model of a deformable porous medium saturated with a multiphase mixture of liquids and gases is required.

For the modelling of seismic waves, the most common approach was proposed by Biot in the middle of the last century and further developed in applications to geophysics [4–6]. Biot's theory is a linear theory of a medium consisting of an elastic porous skeleton and a fluid filling the pores, the equations of which are derived under certain assumptions based on the definitions of the elastic deformation energy density function and the kinetic energy. It predicts three types of waves: fast and slow compressional waves and shear waves, and can be successfully used to study various seismic problems. However, its application to wave modelling for porosities close to 0 and 1 is problematic, and it is also unclear how to generalise the Biot model to the case of finite deformations.

We use an alternative model of small amplitude wave propagation in a saturated porous medium, obtained by simplifying the general symmetric hyperbolic thermodynamically compatible (SHTC) porous medium model [7,8]. The theory of SHTC equations allows to design new mathematically and physically correct models of complex media [9–11]. The governing equations of the SHTC poroelasticity model, in contrast to widely used models of wave processes such as the Biot model [4–6], are applicable in a wide range of porosity variations, including its limits of 0 and 1. The analysis of wave propagation using the SHTC model gives results close to those known from Biot's theory [7]. In addition, the SHTC model provides a direct way of modelling waves in the case where the saturating fluid is a multiphase mixture of liquids and gases [12,13].

In our studies, we assume that thawing permafrost can be interpreted as a poroelastic medium with changing porosity during the transition from solid to liquid phase. This means that, depending on the temperature and pressure within the thawing permafrost, it can either be frozen (solid state) or gradually change to a liquid state (water) as the temperature rises.

Field and laboratory data indicate that there is a relationship between the degree of permafrost thaw and the degree of seismic wave attenuation in such media. We therefore suggest that the main criterion for the degree of permafrost thaw may be an estimate of the degree of seismic wave attenuation in such a medium.

In order to correctly model seismic wave fields in a complex geological environment, transitioning from an elastic medium (ice) to a poroelastic medium

(melting permafrost), and then to a liquid medium (water), it is necessary to be able to qualitatively describe the properties of the seismic wave fields in the model. In particular, it is necessary to know how attenuation mechanisms are taken into account in the SHTC model and whether constant quality factor is ensured throughout the seismic frequency range.

2 SHTC System for Wave Field Simulation in Deformed Saturated Porous Medium

2.1 Governing Equations

This section presents a linear system of first-order partial differential equations for small-amplitude wave propagation, derived from the general SHTC system of governing equations for a saturated deformable porous medium [7,8]. Let us consider a stationary, unstressed porous medium, saturated with fluid, in which the density of the skeleton is ρ_2, and the density of the saturating liquid is ρ_1. Assume that a saturated porous medium is a two-phase solid-fluid mixture with the volume fractions of fluid α_1 and solid $\alpha_2 = 1 - \alpha_1$. The porosity coincides with the volume fraction of the saturating liquid $\phi = \alpha_1$. The following state variables are used for simulation of wave propagation: v_i - the velocity of the mixture, w_i - the relative velocity of the fluid motion relative to the skeleton, p - the pressure of the mixture (the same for both phases), σ_{ij} - the stress deviator in the mixture.

$$\begin{aligned}
&\rho\frac{\partial v_i}{\partial t} + \frac{\partial p}{\partial x_i} - \frac{\partial \sigma_{ik}}{\partial x_k} = F_i,\\
&\frac{\partial w_k}{\partial t} + \left(\frac{1}{\rho_1} - \frac{1}{\rho_2}\right)\frac{\partial p}{\partial x_k} = -\chi w^k,\\
&\frac{\partial p}{\partial t} + K\frac{\partial v_k}{\partial x_k} + \frac{\alpha_1\alpha_2}{\rho}\left(\rho_2 - \rho_1\right)K\frac{\partial w_k}{\partial x_k} = 0,\\
&\frac{\partial \sigma_{ik}}{\partial t} - \mu\left(\frac{\partial v_i}{\partial x_k} + \frac{\partial v_k}{\partial x_i} - \frac{2}{3}\delta_{ik}\frac{\partial v_j}{\partial x_j}\right) = -\frac{\sigma_{ik}}{\tau}.
\end{aligned} \tag{1}$$

The mixture and relative velocities are connected with solid and fluid phase velocities v_2^i and v_1^i as $v_i = c_1 v_1^i + c_2 v_2^i$ and $w_i = v_1^i - v_2^i$ respectively, where $c_1 = \alpha_1\rho_1/\rho$, $c_2 = \alpha_2\rho_2/\rho$ are phase mass fractions and $\rho = \alpha_1\rho_1 + \alpha_2\rho_2$ is the mixture density. The bulk modulus of the mixture K is related to the bulk moduli of the constituents K_1, K_2 by the relation $K = (\alpha_1/K_1 + \alpha_2/K_2)^{-1}$. $\mu = \alpha_2\mu_2$ is the shear modulus of the mixture, μ_2 is the shear modulus of the material of skeleton. F_i defines the external force source exciting the wave field. Right hand side of the equation for the relative velocity w_k contains interphase friction force with the friction coefficient $\chi = c_1c_2/\theta$. In the right hand side of equation for the stress deviator σ_{ik} there is shear stress relaxation term with relaxation time τ.

Our goal is to study the influence of temperature changes on the properties of wave fields based on solving system (1). It is clear that the coefficients in

the equations (material constants) change depending on the temperature. But in the range of its change that interests us, near the melting temperature of ice, the material parameters of the solid and liquid phases change insignificantly, except for the change in porosity. Porosity can rise from 0 significantly as ice melts. Therefore, in what follows we neglect the change in densities and moduli of phases depending on temperature and study the dependence of wave fields only on temperature changes in porosity.

Thus, the list of parameters in (1) which can be a function of porosity $\alpha_1 = \phi$ generated by the temperature variation:

- $\rho = \phi\rho_1 + (1-\phi)\rho_2$ - the total density of the mixture
- $c_1 = \phi\rho_1/\rho_0, c_2 = 1 - c_1 = (1-\phi)\rho_2/\rho$ - phase mass fractions
- $K = (\phi K_1^{-1} + (1-\phi)K_2^{-1})^{-1}$ - the bulk modulus of the mixture
- $\mu = (1-\phi)\mu_2$ - the shear modulus of the mixture
- θ - the relative velocity relaxation time, $\theta^{-1} \sim \eta/k$ (η - viscosity k - permeability)
- τ - shear stress relaxation time

Of course θ and τ depend on porosity. Since we have no available data on this dependence, in this paper we assume that there is no friction $\theta = \infty$ and study the qualitative wave fields behaviour varying τ for different values of porosity.

2.2 Energy Dissipation

The important property of the system (1) is the energy dissipation produced by the source terms. The energy balance equation can be obtained by transforming system (1) to a symmetric form and then deriving the energy integral by multiplying all equations by the appropriate coefficients and summing them up. Below we simply present a final result. The total energy of the medium should be defined as

$$\mathcal{E} = \rho\frac{v_n v_n}{2} + \rho c_1 c_2 \frac{w_n w_n}{2} + \frac{1}{2K}p^2 + \frac{\sigma_{ij}\sigma_{ij}}{2\mu}.$$

Thus, in order to obtain the law of energy balance, it is necessary to multiply the equations of system (1), respectively, by v_i, $\rho c_1 c_2 w_k$, p/K, $\sigma_{ik}/(2\mu)$. Summing everything up, we arrive at the equation

$$\frac{\partial \mathcal{E}}{\partial t} + \frac{\partial\left(pv_k + \rho c_1 c_2\left(\frac{1}{\rho_1} - \frac{1}{\rho_2}\right)pw_k - \sigma_{ik}v_i\right)}{\partial x_k} = -\frac{\rho(c_1c_2)^2 w_n w_n}{2\theta} - \frac{\sigma_{ij}\sigma_{ij}}{2\mu\tau}. \quad (2)$$

In the right hand side of the energy balance Eq. (2) there is a negative source term appeared due to the interphase friction and shear stress relaxation. This source term produces the energy dissipation which causes waves attenuation.

It is important to emphasise that the process of seismic wave attenuation in porous media is a complex phenomenon influenced by various factors such as the structure of the medium, the properties of the fluid and the elastic skeleton, the wave characteristics of the seismic wave and others.

In particular, the main factors leading to the attenuation of seismic energy in the poroelastic medium are internal interfacial friction and stress relaxation. Interfacial friction in porous media refers to the frictional force between different phases in the medium, e.g. between a liquid and a solid phase. Stress relaxation processes are processes in which stresses decrease after the application of an external force. For example, in the context of melting ice, stress relaxation occurs when the ice changes from a solid to a liquid state, resulting in a reduction of stresses in the material. This process is influenced by temperature change and the solid-liquid transition, which together favour stress relaxation in porous media.

Various mathematical models are used to describe the attenuation of seismic energy in the medium, in particular the widely used Generalised Standard Linear Solid (GSLS) model [14], which takes into account both elastic and viscous properties of the medium.

The quality factor (Q-factor) is used to estimate the energy absorption of seismic waves propagating through a medium and is defined as $Q = 2\pi(E/\delta E)$, where $(E/\delta E)$ is the fraction of energy loss per cycle. The assumption of constancy of the seismic Q-factor is fundamental to seismic research. This assumption implies that the Q-factor remains constant over the entire seismic frequency spectrum. The GSLS model is based on the assumption of near constancy of Q, which makes it a proven tool for the study of wave fields in attenuated media.

In order to be confident that our proposed model also provides a constant Q-factor over the seismic frequency range, it is necessary to perform numerical tests.

3 Finite Difference Method

Our numerical approach is based on the staggered grid finite difference method [15,16]. In the context of two dimensions, we introduce new symbols for the coordinates $x = x_1$, $y = x_2$ and the state variables $V_x = V_1$, $V_y = V_2$, $W_x = W_1$, $W_y = W_2$, $\Sigma_{xx} = \Sigma_{11}$, $\Sigma_{yy} = \Sigma_{22}$, $\Sigma_{xy} = \Sigma_{12}$.

Within the (t, x, y) space-time framework, we construct a grid with integer nodes at $t^n = n\Delta t$, $x_i = i\Delta x$, $y_j = j\Delta y$, and semi-integer nodes at $t^{n+1/2} = (n + 1/2)\Delta t$, $x_{i+1/2} = (i + 1/2)\Delta x$, $y_{j+1/2} = (j + 1/2)\Delta y$, where Δt, Δx and Δy represent the grid spacings in time and space.

The staggered grid finite difference method is based on the finite volume discretization method presented in particular in [17], and is often applied to systems of equations derived from physical conservation laws. A key advantage of this approach is that it eliminates the need to approximate fluxes during the solution, as the flux values are known, increasing the efficiency and reliability of the method. As part of this technique, we define the stresses and velocities at different grid points in space and time to provide a second-order accuracy approximation with a minimal difference scheme template.

It is assumed that the material parameters remain constant within each grid cell $[x_{i-1/2}, x_{i+1/2}] \times [y_{j-1/2}, y_{j+1/2}]$, allowing for potential discontinuities along the grid boundaries.

The mixture velocities V_x, V_y and the relative velocities W_x, W_y are defined at specific points $(i+1/2, j)$, $(i, j+1/2)$ and denoted as $(V_x)^n_{i+1/2,j}$, $(V_y)^n_{i,j+1/2}$, $(W_x)^n_{i+1/2,j}$, $(W_y)^n_{i,j+1/2}$.

Pressure and deviatoric stresses are assigned to points (i, j) as $(P)^{n+1/2}_{i,j}$, $(\Sigma_{xx})^{n+1/2}_{i,j}$, $(\Sigma_{yy})^{n+1/2}_{i,j}$, and the shear stress is assigned to the points $(i+1/2, j+1/2)$ as $(\Sigma_{xy})^{n+1/2}_{i+1/2,j+1/2}$. The spatial arrangement of the nodes on the staggered grid is shown in Fig. 1.

For compactness, let us introduce a few notations for a discrete function $f^n_{i,j} = f(t^n, x_i, y_j)$:

– Second-order central difference operators

$$D_t[f]^n_{i,j} = \frac{(f)^{n+1/2}_{i,j} - (f)^{n-1/2}_{i,j}}{\Delta t}, \qquad A_t[f]^n_{i,j} = \frac{(f)^{n+1/2}_{i,j} + (f)^{n-1/2}_{i,j}}{2}, \tag{3}$$

– Fourth-order central difference operators (Levander stencil)

$$D_x[f]^n_{i,j} = \frac{1}{\Delta x}\left\{\frac{9}{8}\left((f)^n_{i+1/2,j} - (f)^n_{i-1/2,j}\right) - \frac{1}{24}\left((f)^n_{i+3/2,j} - (f)^n_{i-3/2,j}\right)\right\}, \tag{4}$$

$$D_y[f]^n_{i,j} = \frac{1}{\Delta y}\left\{\frac{9}{8}\left((f)^n_{i,j+1/2} - (f)^n_{i,j-1/2}\right) - \frac{1}{24}\left((f)^n_{i,j+3/2} - (f)^n_{i,j-3/2}\right)\right\}, \tag{5}$$

– Volumetric arithmetic averaging

$$\langle f\rangle_{i+1/2,j} = (f_{i,j} + f_{i+1,j})/2, \qquad \langle f\rangle_{i,j+1/2} = (f_{i,j} + f_{i,j+1})/2, \tag{6}$$

– Harmonic averaging by [18]

$$\{f\}_{i+1/2,j+1/2} = \left[\frac{1}{4}\left(\frac{1}{f_{i,j}} + \frac{1}{f_{i+1,j}} + \frac{1}{f_{i,j+1}} + \frac{1}{f_{i+1,j+1}}\right)\right]^{-1}. \tag{7}$$

Using these notations, the finite difference equations can be written as

$$\begin{aligned} D_t[V_x]^{n-1/2}_{i+1/2,j} = &-\left\langle 1/\rho^0\right\rangle_{i+1/2,j} D_x[P]^{n-1/2}_{i+1/2,j} \\ &+\left\langle 1/\rho^0\right\rangle_{i+1/2,j}\left(D_x[\Sigma_{xx}]^{n-1/2}_{i+1/2,j} + D_y[\Sigma_{xy}]^{n-1/2}_{i+1/2,j}\right) + [F_x]^{n-1/2}_{i+1/2,j}, \end{aligned} \tag{8}$$

$$\begin{aligned} D_t[V_y]^{n-1/2}_{i,j+1/2} = &-\left\langle 1/\rho^0\right\rangle_{i,j+1/2} D_y[P]^{n-1/2}_{i,j+1/2} \\ &+\left\langle 1/\rho^0\right\rangle_{i,j+1/2}\left(D_x[\Sigma_{xy}]^{n-1/2}_{i,j+1/2} + D_y[\Sigma_{yy}]^{n-1/2}_{i,j+1/2}\right) + [F_y]^{n-1/2}_{i,j+1/2}, \end{aligned} \tag{9}$$

$$\begin{aligned} D_t[W_x]^{n-1/2}_{i+1/2,j} = &-\left\langle 1/\rho^0_1 - 1/\rho^0_2\right\rangle_{i+1/2,j} D_x[P]^{n-1/2}_{i+1/2,j} \\ &-\left\langle c^0_1 c^0_2/\theta_2\right\rangle_{i+1/2,j} A_t[W_x]^{n-1/2}_{i+1/2,j}, \end{aligned} \tag{10}$$

$$D_t[W_y]^{n-1/2}_{i,j+1/2} = -\left\langle 1/\rho_1^0 - 1/\rho_2^0 \right\rangle_{i,j+1/2} D_y[P]^{n-1/2}_{i,j+1/2} - \left\langle c_1^0 c_2^0/\theta_2 \right\rangle_{i,j+1/2} A_t[W_y]^{n-1/2}_{i,j+1/2}, \tag{11}$$

$$D_t[P]^n_{i,j} = -(K)_{i,j}\left(D_x[V_x]^n_{i,j} + D_y[V_y]^n_{i,j}\right) - \left((\rho_2^0 - \rho_1^0)\alpha_1^0\alpha_2^0 K/\rho^0\right)_{i,j}\left(D_x[W_x]^n_{i,j} + D_y[W_y]^n_{i,j}\right), \tag{12}$$

$$D_t[\Sigma_{xx}]^n_{i,j} = (\mu)_{i,j}\left(\frac{4}{3}D_x[V_x]^n_{i,j} - \frac{2}{3}D_y[V_y]^n_{i,j}\right) - (1/\tau)_{i,j}A_t[\Sigma_{xx}]^n_{i,j}, \tag{13}$$

$$D_t[\Sigma_{yy}]^n_{i,j} = (\mu)_{i,j}\left(\frac{4}{3}D_y[V_y]^n_{i,j} - \frac{2}{3}D_x[V_x]^n_{i,j}\right) - (1/\tau)_{i,j}A_t[\Sigma_{yy}]^n_{i,j}, \tag{14}$$

$$D_t[\Sigma_{xy}]^n_{i+1/2,j+1/2} = \{\mu\}_{i+1/2,j+1/2}\left(D_x[\Sigma_y]^n_{i+1/2,j+1/2} + D_y[V_x]^n_{i+1/2,j+1/2}\right) - \{1/\tau\}_{i+1/2,j+1/2}A_t[\Sigma_{xy}]^n_{i+1/2,j+1/2}. \tag{15}$$

The scheme obtained is an explicit finite difference scheme of second order accuracy in time and space for a homogeneous elastic medium. Stability conditions and dispersion properties can be found in [15].

4 Numerical Test Problem

As mentioned above, the correct behaviour of the seismic wave fields described by system (1) should ensure a constant Q-factor over the range of seismic frequencies.

The wave attenuation mechanisms included in system (1) are taken into account by introducing two right-hand terms into the equations for the relative velocities w_i and for the stress deviator σ_{ik}.

The first term corresponds to the interfacial frictional force with the friction coefficient $\chi = c_1 c_2/\theta$. The second term corresponds to the shear stress relaxation with relaxation time τ.

Preliminary calculations have shown that interphase friction mainly attenuates the slow P-wave (Biot wave), while the term responsible for shear stress relaxation affects the attenuation of the fast P- and S-waves. In the seismic frequency range, the slow P-wave attenuates rapidly and its amplitude becomes negligible, so this wave may not be taken into account when interpreting seismic data. For this reason, we focus on the mechanism of shear stress relaxation and its effect on wave attenuation, assuming $\chi = 0$ in further calculations.

Consider a homogeneous poroelastic medium with the material parameters given in Table 1. We assume that the thawing permafrost can be considered as a poroelastic medium with varying porosity. Depending on the temperature and pressure within the thawing permafrost, it may be either frozen (solid state) or in the process of transitioning to a liquid state (water) as the temperature rises.

In the frozen state, i.e. ice, it can be considered as a limiting case of poroelastic medium by setting the porosity (equal to the volume fraction of liquid $\phi = \alpha_1^0$) to 0 in system (1). During the melting process, the porosity of the medium increases to the value of the pure liquid state $\phi = 1$.

The calculations were carried out for the domain (800×800) m. The wave field is excited by a vertical type source with $F_x(x, y, t) = 0$ and $F_y(x, y, t) = \delta(x_0, y_0) f(t)$, where δ is the Dirac delta function that locates the source in the centre of the domain $(x_0, y_0) = (400, 400)$ m. The time function $f(t)$ is given by the Ricker wavelet $f(t) = (1 - \omega^2 (t - t_0)^2/2) exp[-\omega^2 (t - t_0)^2/4]$ with dominated frequency $f_0 = 150$ Hz ($\omega = 2\pi f_0$) and pulse delay $t_0 = 2/f_0$.

Figure 2 shows snapshots of the wave field simulation for a homogeneous poroelastic medium taken at time $t = 0.1$ seconds for different porosities $\phi = 0, \phi = 0.5$ and $\phi = 1$.

As can be seen from the plots in Fig. 2, the wave field varies significantly depending on the porosity of the medium. In the case of porosity $\phi = 1$ we have a pure liquid medium. In such a medium there is only a pressure wave propagating with the velocity of the fluid phase 1500 m/s. In the case of porosity $\phi = 0$ we have a pure elastic medium with a longitudinal and a shear wave propagating with velocities of 3800 m/s and 2400 m/s respectively. And in the case of porosity $\phi = 0.5$, together with longitudinal and shear waves, we see the appearance of a slow Biot wave in the poroelastic medium. The velocity of these waves depends on the frequency of the signal at the source and can be estimated using dispersion curves.

The next step was to perform a series of numerical simulations to estimate the quality factor Q (Q-factor). Several approaches are known to estimate the Q-factor, expressing the value in terms of elastic moduli, energies, spatial attenuation coefficient, phase delay between stress and strain, signal amplitude, etc. [19]. Since in our experiment we perform wave propagation and have the possibility to record the signal by receivers, we adopt a signal deconvolution approach [20]. Considering two receivers at points $y = y_1$ and $y = y_2$ located on the same vertical line passing through the source, we obtain two traces for P-waves propagating over the distance d_0 and $d_0 + d$. We consider the signal propagating at the receiver closer to the source to be of the form $u_1 = u_0 e^{i\omega(t - y_1/c(\omega))}$, where u_0 is the amplitude and $c(\omega)$ is the complex phase velocity. After propagation over the distance d, the expression for the wave takes the form $u_2 = u_1 e^{i\omega d/c(\omega)}$. The transition to the frequency domain using the Fourier transform is applied to the signals u_1 and u_2 to deconvolve them by the ratio u_2/u_1. The components $c(\omega)$ are then obtained from the logarithm of the ratio of the signals, and the quality factor can be estimated by $Q = \lambda Re(c^2)/Im(c^2)$, where λ is the wavelength. In order to obtain an estimate that is independent of the distance between the two receivers, a multiplication by the wavelength is carried out.

Calculations were carried out for different values of porosity and different values of relaxation time. The results are shown in Figs. 3-7. Figure 3 shows the estimation of the Q-factor for a purely elastic medium with porosity $\phi = 0$ and for different relaxation times τ. The estimation is performed for the seismic frequency range 70–300 Hz. The graph shows that for all relaxation times considered, the Q-factor is the same and equal to the constant 560. This value corresponds to a medium in which there is practically no attenuation.

The situation changes when the medium becomes porous. Figures 4-7 show the evaluation of the Q-factor for the medium with different porosities $\phi = 0.8$, $\phi = 0.5$, $\phi = 0.2$, $\phi = 0$. Since we do not have data on the dependence of the relaxation time on the porosity, a series of calculations were made for each porosity and for different relaxation times $\tau = \infty$, $\tau = 0.1$, $\tau = 0.05$, $\tau = 0.01$, $\tau = 0.005$.

Comparing the graphs, it can be seen that for porous media the relaxation time τ begins to play a significant role in the magnitude of seismic wave attenuation. Simultaneously, the analysis of the numerical results confirms that system (1) ensures the consistency of the Q-factor in the seismic frequency range for all porosity and relaxation time values.

Note that τ in system (1) is very similar to the τ parameter in the τ-method used to simulate the behaviour of viscoelastic materials in viscoelastic models such as the Standard Linear Solid (SLS) and the Generalised Standard Linear Solid (GSLS) models [21,22]. In the τ-method, this parameter characterises the time-dependent response of viscoelastic materials to applied stress and is introduced to save memory, replacing the need to introduce stress and strain relaxation times separately for each of the P and S waves in the SLS and GSLS models.

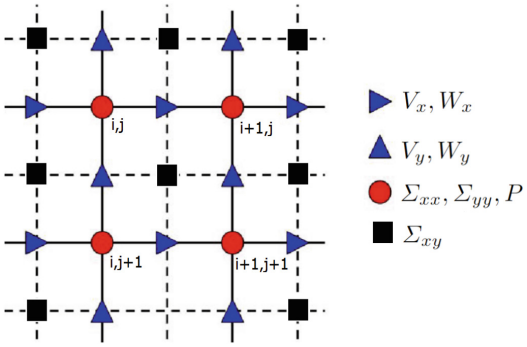

Fig. 1. The relative position of deviatoric stresses, pressure, mixture velocities and relative velocities on the staggered grid.

Table 1. Material parameters of the media.

State	Parameter	Notation	Value	Unit
Solid phase	Longitudinal sound velocity	V_p	3800	m/s
	Shear sound velocity	V_s	2400	m/s
	Density	ρ_2	2500	kg/m^3
Fluid phase	Longitudinal sound velocity	V_p	1500	m/s
	Shear sound velocity	V_s	0	m/s
	Density	ρ_2	1040	kg/m^3
Dissipative parameters	Interphase friction	$c_1^0 c_2^0/\theta_2$	–	s^{-1}
	Relaxation time	τ	10^{-2}	s

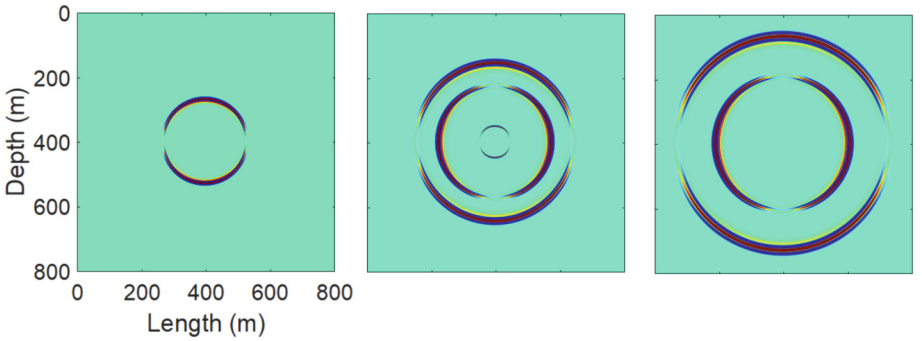

Fig. 2. Snapshot of the mixture velocity component $u2$, recorded for relaxation time $\tau = \infty$ and porosity $\phi = 1$ (left), $\phi = 0.5$ (middle), $\phi = 0$ (right) at time 0.1 s.

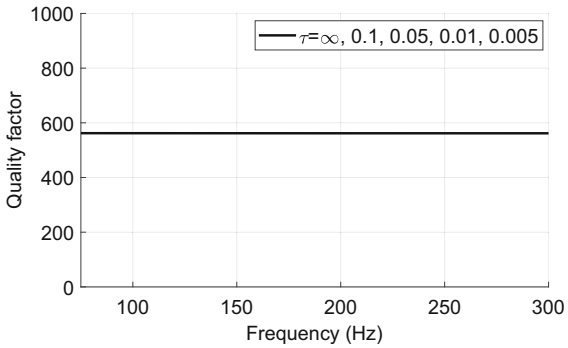

Fig. 3. Compare Q-factor for porosity $\phi = 0$ and different relaxation times in seismic frequency band 70–300 Hz.

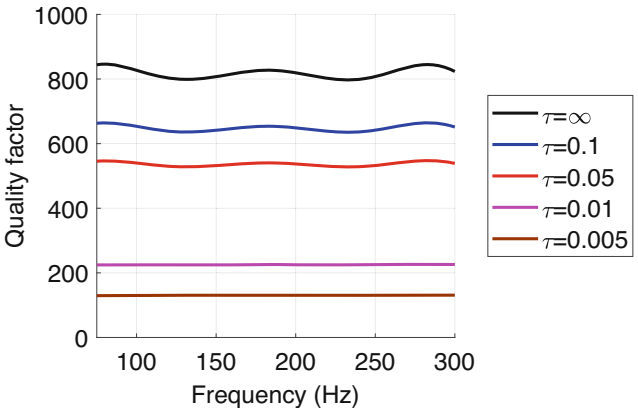

Fig. 4. Compare Q-factor for porosity $\phi = 0.8$ and different relaxation times in seismic frequency band 70–300 Hz.

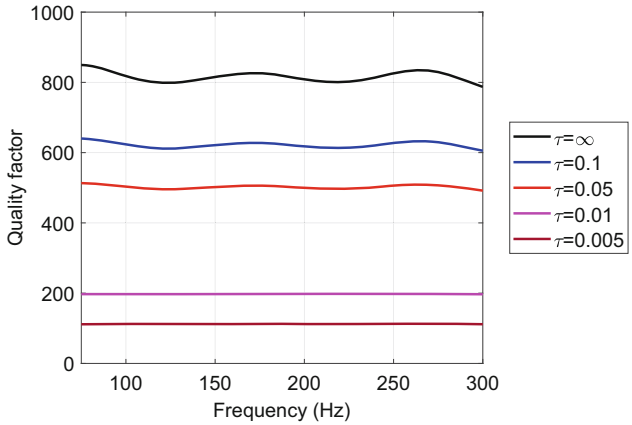

Fig. 5. Compare Q-factor for porosity $\phi = 0.5$ and different relaxation times in seismic frequency band 70–300 Hz.

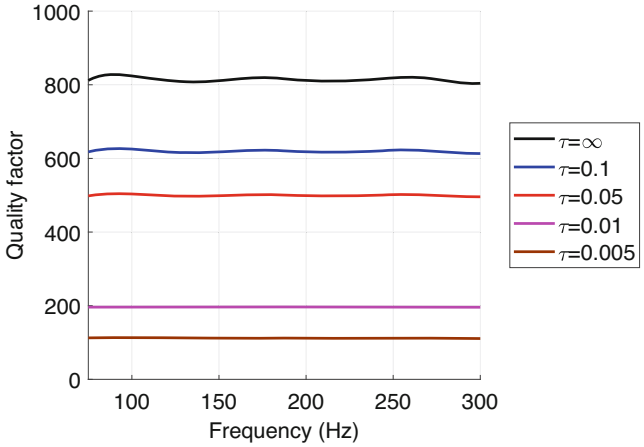

Fig. 6. Compare Q-factor for porosity $\phi = 0.2$ and different relaxation times in seismic frequency band 70–300 Hz.

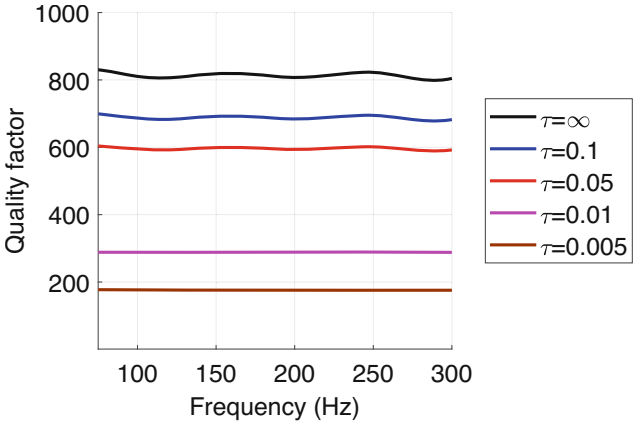

Fig. 7. Compare Q-factor for porosity $\phi = 1$ and different relaxation times in seismic frequency band 70–300 Hz.

5 Conclusions

To study the effect of temperature changes on wave fields during permafrost thawing, a Symmetric Hyperbolic Thermodynamically Compatible (SHTC) model of a saturated porous medium is used, designed to describe the propagation of small amplitude waves. The efficient finite difference method on staggered grid is applied to solving a series of two-dimensional test problems. Although all material parameters in the governing equations may depend on temperature variations, it is shown numerically that wave attenuation and energy dissipation are mainly caused by the dependence of the relaxation time of shear stresses on porosity, the growth of which is due to the thawing of permafrost with a change in temperature. To estimate the energy dissipation during seismic waves propagation the quality factor is used. Since there is no data on the dependence of shear stress relaxation time on porosity, a series of calculations were carried out for different values of porosity and relaxation time. It is concluded that an increase in porosity, accompanied by a decrease in relaxation time, leads to an increase in the quality factor, that is, it increases the absorption of seismic waves. This fact may be the basis for the development of seismic methods for monitoring permafrost thawing.

References

1. Guillemot, A., et al.: Seismic monitoring in the Gugla rock glacier (Switzerland): ambient noise correlation, microseismicity and modelling. Geophys. J. Int. **221**(3), 1719–1735 (2020)
2. Albaric, J., Kühn, D., Ohrnberger, M., Langet, N., Harris, D., Polom, U., et al.: Seismic monitoring of permafrost in Svalbard Arctic Norway. Seismological Res. Lett. **92**(5), 2891–2904 (2021)

3. Steinmann, R., Hadziioannou, C., Larose, E.: Effect of centimetric freezing of the near subsurface on Rayleigh and Love wave velocity in ambient seismic noise correlations. Geophys. J. Int. **224**(1), 626–636 (2021)
4. Biot, M. A.: Theory of propagation of elastic waves in fluid-saturated porous solid. I. Low-frequency range. J. Acoust. Soc. Am. **28**(2), 168–178 (1956)
5. Biot, M. A.: Theory of propagation of elastic waves in a fluid-saturated porous solid. II. Higher frequency range. J. Acoust. Soc. Am. **28**(2), 179–191 (1956)
6. Carcione, J.M., Morency, C., Santos, V.: Computational poroelasticity - a review. Geophysics **75**(5), 75A229-75A243 (2010)
7. Romenski, E., Reshetova, G., Peshkov, I., Dumbser, M.: Modeling wavefields in saturated elastic porous media based on thermodynamically compatible system theory for two-phase solid-fluid mixtures. Comput. Fluids **206**, 104587 (2020)
8. Reshetova, G., Romenski, E.: Diffuse interface approach to modeling wavefields in a saturated porous medium. Appl. Math. Comput. **398**, 125978 (2021)
9. Godunov, S.K., Romenskii, E.I.: Elements of continuum mechanics and conservation laws. Springer, New York, NY (2003). https://doi.org/10.1007/978-1-4757-5117-8
10. Romenski, E.: Hyperbolic systems of thermodynamically compatible conservation laws in continuum mechanics. Math. Comput. Modell. **28**, 115–130 (1998)
11. Peshkov, I., Pavelka, M., Romenski, E., Grmela, M.: Continuum mechanics and thermodynamics in the Hamilton and the Godunov-type formulations. Continuum Mech. Thermodyn. **30**, 1343–1378 (2018)
12. Romenski, E., Reshetova, G., Peshkov, I.: Computational model for compressible two-phase flow in deformed porous medium. In: Gervasi, O., et al. (eds.) ICCSA 2021. LNCS, vol. 12949, pp. 224–236. Springer, Cham (2021). https://doi.org/10.1007/978-3-030-86653-2_16
13. Romenski, E., Reshetova, G., Peshkov, I.: Two-phase hyperbolic model for porous media saturated with a viscous fluid and its application to wavefield simulation. Appl. Math. Model. **106**, 567–600 (2022)
14. Carcione, J.M., Kosloff, D., Kosloff, R.: Wave propagation simulation in a linear viscoacoustic medium. Geophys. J. Int. Geophys. **93**(2), 393–401 (1988)
15. Virieux, J.: P-SV wave propagation in heterogeneous media: velocity-stress finite-difference method. Geophysics **51**(1), 889–901 (1986)
16. Graves, R.W.: Simulating seismic wave propagation in 3D elastic media using staggered- grid finite differences. Bull. Seismol. Soc. Am. **86**(4), 1091–1106 (1996)
17. Samarskii, A.A.: The theory of difference schemes. CRC Press, Boca Raton (2001)
18. Moczo, P., Kristek, J., Vavrycuk, V., Archuleta, R.J., Halada, L.: 3d heterogeneous staggered-grid finite-difference modeling of seismic motion with volume harmonic and arithmetic averaging of elastic moduli and densities. Bull. Seismol. Soc. Am. **92**(8), 3042–3066 (2002)
19. Mavko, G., Mukerj, T., Dvorkin, J.: The Rock Physics Handbook, 2nd edn. Cambridge University Press, Cambridge (1999)
20. Caspari, E., et al.: Attenuation mechanisms in fractured fluid-saturated porous rocks: a numerical modelling study. Geophys. Prospect. **67**(4), 935–955 (2019)
21. Blanch, J., Robertsson, O., Symes, W.: Modeling of a constant Q: methodology and algorithm for an efficient and optimally inexpensive viscoelastic technique. Geophysics **60**, 176–184 (1995)
22. Hestholm, S., et al.: Quick and accurate Q parameterization in viscoelastic wave modeling. Geophysics **71**(5), T147–T150 (2006)